Supplementary Materials

Motivations for each measure

In this section we provide a detailed description of the motivations for each measure used in this study. For details of the computations see the supplementary methods.

Event Related Potentials

The auditory protocol (Bekinschtein et al., 2009) was originally designed to elicit and isolate early and late event-related potentials (ERPs). Recent theories of consciousness indeed argue that early components correspond to unconscious processing stages, whereas late components are associated with conscious access (see review in (Dehaene et al., 2006; Sergent and Naccache, 2012)). In addition to early auditory P1 and N1 components, our auditory protocol allows identifying three responses related to the detection and the expectation of an auditory novelty: the contingent negative variation (CNV), the mismatch negativity (MMN) and the P3b component.

The CNV is a slow negative drift generally observed over the frontal electrodes when subjects expect an informative stimulus and terminates when such stimulus is presented (Walter et al., 1964). This component is believed to be generated by a large network and necessitate subjects to be attentive and actively engaged in the task (Rosahl and Knight, 1995; Niedermeyer, 2003; Gómez et al., 2007; Chennu et al., 2013). As these two conditions are generally associated with conscious perception (Dehaene et al., 2006; Dehaene and Changeux, 2011) the CNV could sensitively mark a conscious state. Indeed, in a similar experimental protocol, Faugeras et al (Faugeras et al., 2012) has observed a negative drift ranging from the first to the last sound of each trial, proved which distinguished patients in various states of consciousness (Walter et al., 1964; Faugeras et al., 2012).

The MMN is elicited by a change in pitch in the last of the five tones (XXXXX versus XXXXY) (Näätänen et al., 1978). This component has been repeatedly reported under non-conscious conditions, although its amplitude can be modulated by subjects' attention (Bekinschtein et al., 2009) and conscious state (in sleep (Nashida et al., 2000) and in DOC patients (Fischer et al., 2004, 2010; Naccache et al., 2005; Kotchoubey et al., 2005; Wijnen et al., 2007; Bekinschtein et al., 2009; Schnakers et al., 2009; Morlet and Fischer, 2013) .

The P300b (P3b) component is observed across a wide variety of tasks and is generally elicited by visible relevant target (e.g. (Squires et al., 1975; Sergent et al., 2005; Polich, 2007)). This component is believed to reflect a large activation of the fronto-parietal cortices, and has thus been repetitively linked to working memory updating processing (Polich, 2007) and conscious access (Dehaene and Changeux, 2011). Specifically in the present experimental protocol, the P300 response to unexpected (rare) sound sequences has only been observed in conscious and attentive subjects (Bekinschtein et al., 2009; Faugeras et al., 2011, 2012).

Ongoing activity

The rest of our measures were derived from the EEG activity preceding the onset of the last sound (early time window on Figure 1). We refer to this time periods as "ongoing activity". It should be noted however that neutral auditory stimuli were presented during these time periods, which are thus different from traditional resting state conditions. However, we reasoned that it may be possible to quantify the "ongoing" EEG activity that dominates over evoked responses by approximately one order of magnitude. Furthermore, one should note that classical resting state conditions are generally uncontrolled stimulation conditions. Finally, the controlled auditory stimulations here limit drowsiness by repeatedly calling the patient's attention, and could thus help to differentiate MCS from VS patients.

"Ongoing" EEG measures were organized according to two dimensions: i) whether they capture local dynamics or connectivity; and ii) whether their theoretical background lies in a spectral decomposition of the EEG signal, or in information theory.

Measures of EEG spectrum

Local dynamics refer to measures computed within a given EEG electrode. At this level, spectral measures are traditionally applied to quantify EEG oscillations or broadband frequency patterns, many of which have been proposed to distinguish conscious states in anesthesia (Supp et al., 2011), sleep (Finelli et al., 2001) and DOC patients (Fellinger et al., 2011; Fingelkurts et al., 2012). A classical finding is that unconscious subjects, compared to conscious ones, exhibit a reduction in power in the alpha band (8-13 Hz) and an increase in low frequencies such as the delta band (1-4 Hz). In our dataset we estimated power in five frequency bands (delta to low gamma). Frequency analyses were supplemented with spectrum summary measures that summarize the distribution of power over various frequencies using a single value, for instance its median or its spectral entropy (SE, characterizing the complexity of the spectrum). These measures of spectrum summaries have been previously used to characterize the EEG recordings of DOC patients (Schnakers et al., 2008; Gosseries et al., 2011) and subjects under anesthesia (Vakkuri et al., 2004; Velly et al., 2007; Laitio et al., 2008).

Measures of complexity

Novel techniques from the fields of dynamical systems and information theory also provide insights into normal and perturbed neural mechanisms (Dimitrov et al., 2011). These measures can be used to detect characterize changes in the EEG that may not be unveiled using traditional spectral frequency content methods (Stam, 2005).

We included a representative set of information theory measures of local dynamics. In particular, permutation entropy (PE) is an increasingly used method to detect dynamical changes in a time series (Cao et al., 2004), which is known for its high resistance to low signal-to-noise ratios compared to other similar methods (Bandt and Pompe, 2002). PE has been successfully applied to the EEG-based detection of loss of consciousness under anesthesia (Li et al., 2008; Jordan et al., 2008). As described in detail below, PE estimates the entropy of a signal transformed into a sequence of discrete "symbols". These symbols are generated from the qualitative (i.e. ranking) up and downs of the signal.

We introduce an original method to quantify the complexity of EEG signals based on the application of the Kolmogorov-Chaitin complexity (K). This measure quantifies

the algorithmic complexity (see (Kolmogorov, 1965; Chaitin, 1974)) of a single sensor's EEG by measuring his degree of redundancy. Algorithmic complexity of a given string (in this case an EEG sequence) can be described as the length of shortest computer that can generate it. A short program corresponds to a less complex sequence. We estimated K by quantifying the compression size of the EEG using variants of the Lempel-Ziv zip algorithm (Lempel and Ziv, 1976). This measure has been previously applied to detect changes in the cortical activity in anesthetized animals (Shaw et al., 1999) and more recently to index conscious state in human subjects from the evoked response to a TMS pulse (Casali et al., 2013).

Measures of information sharing

Connectivity, in the sense of information sharing across distant cortical areas, has been proposed as a key element of several theories of consciousness (Baars, 1993; Rees et al., 2002; Tononi, 2008; Dehaene and Changeux, 2011). Recent advances in theoretical neuroscience have shown that long-distance communication could be marked (Gaillard et al., 2009; Dehaene and Changeux, 2011) or established (Fries, 2005; Saalmann et al., 2012) by a frequency-specific synchronization across different brain areas (Fries, 2005). Intracranial recordings and M/EEG comparing neural processing elicited by subliminal and visible images revealed an association between conscious perception and long-range synchrony in the beta and gamma bands (Gross et al., 2004; Gaillard et al., 2009; Hipp et al., 2011). Moreover, recent EEG studies suggest that VS patients present lower functional connectivity than MCS and CS patients (Lehembre et al., 2012; Fingelkurts et al., 2012). In the present study, we evaluated synchrony with two traditional spectral methods: phase lag index (PLI) and the imaginary part of coherence (ICOH). The two measures were favored over as they are robust to volume conduction, common source and muscular and eye movements artefacts (Nolte et al., 2004; Stam et al., 2007).

However, such spectral methods are poorly sensitive to non-oscillatory functional connectivity. To address this issue, we also computed an original method for quantifying information sharing: weighted symbolic mutual information (wSMI). wSMI can robustly quantify non-oscillatory functional connectivity by transforming the EEG signals into symbolic sequences and estimating the non-trivial association of symbols across sensors. In a previous study, we have successfully applied wSMI to distinguish vegetative from minimally conscious and conscious states patients (J.-R. King et al., 2013).

Mean value versus fluctuations across trials

For all measures, we introduced a final distinction between their average value and their fluctuation across time (computed as the standard deviation across trials). First, over the course of an hour, vegetative state patients, and a fortiori minimally conscious state patients are believed to present a strongly fluctuating state of vigilance and attention (Laureys et al., 2004). Measuring the fluctuation of each EEG marker may thus help distinguishing different states of consciousness. Second, fluctuation proved to capture independent information from the BOLD signal in a recent fMRI experiment (Garrett et al., 2010). As a consequence, we studied both the mean (μ) and standard deviation (σ) of each measure across trials.

Supplementary methods

Auditory stimulation

Each trial was composed of a series of five 50-ms duration sounds presented via headphones with an intensity of 70 dB and a 100ms interval between each sound (stimulus onset asynchrony [SOA] = 150 ms). Each sound was composed of three superimposed sinusoidal tones (either a low-pitched sound composed with a mixture of 350, 700 and 1400 Hz tones, hereafter sound X; or a high pitched sound composed with a mixture of 500, 1000 and 2000 Hz tones, hereafter sound Y). Tones were prepared with 7ms rise and 7ms fall times. Four different series of sounds were used, the first two using the same five sounds: XXXXX or YYYYY (hereafter denoted as XX); and the other two with the final sound differing from the four other: XXXXY or YYYYX (hereafter denoted as XY). Trials were separated by a variable interval of 1350–1650ms (50ms steps). Blocks were arranged to contain the XY trials, either as a rare (block type 1: 80% XX/20% XY); or as a frequent (block type 2: 80% XY/20% XX) series of sounds. Both blocks presented a local (the fifth sound could be deviant or identical to previous sounds) and a global regularity (one of the series of sounds was rarer than the other). In order to unambiguously establish the global regularity, each block started with 30 second habituation time period during which only trials with series of sounds of the frequent type were presented. Following the original design (Bekinschtein et al., 2009), frequent trials following a rare auditory sequence were discarded from the analyses. This was done to exclude standard trials which may be partially processed as novel within a short time-window. The number of rare trials was pre-selected by the experimenter before the beginning of the recording (between 22 and 30). In most cases the number of rare trials was 26. The proportion of rare trials was kept fixed at 20%. Auditory stimuli were presented with Eprime v1.1 (Psychology Software Tools Inc., Pittsburgh, PA). Instructions to pay attention to the stimuli and to count deviant stimuli were delivered verbally to all patients at the beginning of each block. All subjects performed eight blocks (each block lasting 3 to 4 minutes) in a fixed order (two runs of XX, YY, XY, YX frequent stimulation).

Computation of measures

In this section we describe the procedures applied to compute all measures.

Event-Related Potentials (ERPs)

Mid-latency auditory potential corresponding to the first sound (P1)

In the present study, the P1 was computed by averaging the voltage of a cluster of 7 EEG electrodes surrounding Fz (electrodes [15, 22, 14, 6, 7, 16, 23] in the EGI 256-electrode net) between 68 ms and 116ms following the onset of the first sound and across all trials.

Contingent Negative Variation (CNV)

Following previous methods (#e.g. (Faugeras et al., 2012)), the CNV was computed by averaging the slope of the EEG electrodes' voltage observed between the onset of the 1st sound to the onset of the 5th sound (Linear regression, from 0 to 600 ms). For univariate analyses, the CNV was summarized as the average slope of a cluster of 7 EEG electrodes surrounding Fz (electrodes [15, 22, 14, 6, 7, 16 and 23] in the EGI net).

P3a

Following previous findings (#e.g. (Bekinschtein et al., 2009; Morlet and Fischer, 2013)), the P3a component was computed by averaging the EEG electrodes' voltage between 280 ms to 340 ms following the onset of the 5th sound and across local deviant trials only (XXXXY). For univariate analyses, the P3a was summarized as the average voltage of a cluster of 7 EEG electrodes surrounding Fz (electrodes [15, 22, 14, 6, 7, 16 and 23] in the EGI net)

P3b

Following previous findings (e.g. (Bekinschtein et al., 2009; Faugeras et al., 2012; J. R. King et al., 2013)), the P3b component was computed by averaging the EEG electrodes' voltage between 400 ms to 600 ms following the onset of the 5th sound and across global deviant trials only (rare sequences). For univariate analyses, the P3b was summarized as the average voltage of a cluster of 5 EEG electrodes surrounding Cz (electrodes [9, 186, 132, 81 and 45] in the EGI net).

Mismatch negativity (ΔMMN) and Contrasted P3a (ΔP3a)

The MMN was estimated by contrasting the local deviant trials (LD = XXXXY) versus the local standard trials (LS = XXXXX). Each subjects' MMN was thus summarized as the 256-electrode topography of the LD/LS difference in the time window between 140 ms to 192 ms after the onset of the 5th sound. For the univariate analysis, this value was averaged over a subset of electrodes around Fz and Cz (electrodes [15, 22, 14, 6, 7, 16, 23, 9, 186, 132, 81 and 45] in the EGI net)

Similarly, the ΔP3a was estimated using the same contrast than for the MMN but averaging a time window from 280 ms to 340 ms after the onset of the 5th sound. The same electrodes as for the MMN were used for the univariate analysis.

Contrasted P3b (ΔP3b)

The ΔP3b was contrasted between the rare global deviant (GD) trials and the frequent global standard (GS) trials (Bekinschtein et al., 2009). Each subjects' ΔP3b was then summarized as the 256-electrode topography of the GD/GS difference in the time window between 400 ms to 600 ms after the onset of the 5th sound. For the univariate analysis, this difference was averaged over a subset of electrodes around Cz and Pz (electrodes [9, 186, 132, 81, 45, 101, 100, 129, 128, 119 and 110] in the EGI net) Following the Local Global protocol (Bekinschtein et al., 2009), the late P3b component was isolated by contrasting frequent and expected auditory sequences to rare and thus unexpected auditory sequences. For instance, in a given block, subjects were repeatedly presented with XXXXY trials. On rare occasions (20%), an XXXXX sequence was presented. In another block, subjects were frequently presented with XXXXX, and rarely with XXXXY. Contrasting rare and frequent trials is thus orthogonal to the local change in pitch within a given sequence.

Decoding the MMN and P300b

As patients often present significant brain and skull lesions, they may present a extremely variable topographies from one subject to another. Following a previous study (J. R. King et al., 2013), we thus implemented multivariate pattern classifiers (MVPA), using a linear kernel support vector machine, to optimize the detection of ΔMMN and ΔP300 effects. The MVPA can indeed identify the topographies that best discriminate standard and deviant trials for each subject separately.

Two types of classifiers were trained: (1) local standard versus local deviant ('local classification', similar to ΔMMN); (2) global standard versus global deviant ('global classification', similar to ΔP300).

A standard ten-fold stratified cross-validation was implemented to avoid over-fitting and circular analysis (Kriegeskorte et al., 2009; Vul et al., 2009). In each fold, a support vector classifier (SVC) (Chang and Lin, 2001) was fitted to the training set and supplemented with a probabilistic output method (Platt, 1999). This continuous classification method was then assessed on its ability to accurately predict the class of the test set.

The amplitude of each electrode at multiple time points was provided to the classifier. To minimize the number of irrelevant features, a time window of interest was used for each classification: Local: [0, 367]; Global: [367,736] ms after the onset of the last sound. Each trial was then transformed into a p-dimensional vector x, in which each coordinate corresponds to a single data sample at a given sensor (p =nsensors . ntime samples). The entire dataset can hence be represented as a matrix X in which each row i corresponds to one trial xi, and each column corresponds to one attribute. All data were normalized $(x - \mu(x_{train}))/\sigma(x_{train})$ across all artefact-free trials in each sample of each sensor. Following a previous study, univariate feature selection was performed with a fixed rate of 10%. The SVC was fitted to find the linear hyperplane w that best separate standard from deviant trials. To minimize imbalance effects, sample weights were applied in proportion of the trial local and global classes (frequent xxxx & xxxY; rare xxxx & xxxY) so that each category equally affects the fitting of the hyperplane. Finally, a cumulative probability distribution function was then fitted to the training set using Platt's method (Platt, 1999). The signed distance of the dot product x *w can thus be used to determine the probability of a given trial to belong to the deviant class. Finally, classification scores, summarized with the area under the curve (AUC), were estimated from the predicted probabilities of the trials from the testing set. All multivariate analyses were performed with the Scikit-learn toolbox (Pedregosa et al., 2011).

Local dynamics (within electrodes)

Spectral analysis

Power spectral density on each trial was estimated using the Welch method (Welch, 1967). For each trial, each electrode was divided in 500-ms sections with 400 ms of overlap. Sections were windowed with a Hamming window and zero padded to 4096 samples. The power in each frequency band was calculated as the integral of the power spectral density (PSD) within each frequency bands, and finally log scaled. Frequency-bands of interest were: Delta (δ: 1-4 Hz), Theta (θ: 4-8 Hz), Alpha (α: 8-13 Hz), Beta (β: 13-30 Hz) and Gamma (γ: 30-45 Hz). Higher frequencies were not estimated as they are generally difficult to measure in an artifact-free manner with scalp EEG. Multitaper analyses (Mitra and Bokil, 2007) revealed similar phenomena to the Welch method. However, as they do not easily provide a single trial estimates, we opted to only report Welch results.

Estimation of the PSDs can be influenced by several phenomena (e.g. electrode impedances, eye movements, etc.) creating inter-individual variance in the absolute EEG power. To bypass this problem, following the method proposed in (Vogt et al.,

1998), normalized powers were also estimated by dividing the power in each band by the total energy in the trial (thus setting the total power in the five frequency bands to 100%). These estimates are referred to δ_n, θ_n, α_n, β_n, and γ_n respectively.

Spectral summaries

Power spectrum centroids (MSF, SEF)

Spectral summaries were estimated using the following measures: median power frequency (MSF), spectral edge 90 (SEF90) and spectral edge 95 (SEF95) (reviewed in (Rampil, 1998)). These measures are defined as the particular frequencies that divide the power spectrum into two parts of equal area (MSF), a lower part equal to 90% of the total area and a higher part equal to 10% (SEF90), or a lower part equal to 95% of the total area and a higher part equal to 5% (SEF95).In all cases, these measures were estimated using the power spectral density for each electrode in each trial.

Spectral entropy (SE)

The entropy of a time series is a measure of signal predictability and is thus a direct estimation of the information it contains (MacKay, 2003). Entropy can be measured in the time domain but also in the spectral domain. Spectral entropy basically quantifies the amount of organization of the spectral distribution (Inouye et al., 1991). We implemented the spectral entropy (SE) measure using the algorithm described for anesthesia monitors (Viertiö-Oja et al., 2004). The SE index for each electrode in each trial was estimated with the following procedure: i) the power spectral density of each trial was normalized (PSD_n) by dividing it by the total energy in that trial; ii) SE was calculated, using the Shannon Entropy formula for all frequency bins (f):

$$SE = -\sum_{f} PSD_n(f)\ \log(PSD_n(f)\ )$$

Signal complexity

Permutation entropy

Permutation entropy (PE), introduced by Bandt & Pompe (Bandt and Pompe, 2002), is an effective method to compare time series and distinguish different types of behavior (e.g. periodic, chaotic or random). One key feature of the method is its robustness to low signal to noise ratios compared to other similar methods (Bandt and Pompe, 2002). The basic principle of this method is the transformation of the time signal into a sequence of symbols before estimating entropy. The transformation is made by considering consecutive sub-vectors of the signal of size n. These sub-vectors can be made of either consecutive elements or of elements separated by τ samples (where τ is an integer). The τ parameter thus defines a broad frequency-specific window of sensitivity for this measure (see Figure S1 for the spectral sensitivity of the method given the present parameters). Since using τ values larger than 1 induce aliasing effects, the signal was low-pass filtered before PE calculation, in order to maintain the frequency-band specificity of each measure. Cutoff frequencies were set according to the following formula: $f_{LP} = \frac{80\ Hz}{\tau}$, appropriate given our sampling rate . Each sub-vector of length n is associated with a unique symbol, based solely on the ordering of its n signal amplitudes. Given the parameter n there are $n!$ possible vectors, corresponding to distinct categories of signal variations. After the symbolic transform, the probability of each symbol is estimated, and PE is computed by applying Shannon's classical

formula to the probability distribution of the symbols. In our case we computed PE for every electrode and in every trial with parameters n = 3 and τ = [8, 4, 2, an 1], corresponding respectively to PE_θ, PE_α, PE_β and PE_γ respectively. Repeating the analysis with n = 4 yielded very similar results. However PE becomes harder to robustly estimate for larger n values, because the size of the estimated probability matrix increases rapidly.

Kolmogorov Chaitin complexity

Algorithmic information theory has been introduced by Andreï Kolmogorov and Gregory Chaitin as an area of interaction between computer science and information theory. The concept of algorithmic complexity or Kolmogorov-Chaitin complexity (K) is defined as the shortest description of a string (or in our case a time series). That is to say, K is the size of the smallest algorithm (or computer program) that can produce that particular time series. However, it can be demonstrated by *reductio ad absurdum* that there is no possible algorithm that can measure K (Chaitin, 1995). To sidestep this issue, we can estimate an upper-bound value of K(X). This can be concretely accomplished by applying a lossless compression of the time series and quantifying the compression size. Capitalizing on the vast signal compression literature, we heuristically used a classical open-source compressor gzip (Salomon, 2007) to estimate K (X). It is important to normalize the method of representation of the signal before compression in order to avoid non-relevant differences in complexity. To compute K(x)

- (1) the time series were transformed into sequences of symbols. Each symbol represents, with identical complexity, the amplitude of the corresponding channel for each time point. The number of symbols was set to 32 and each one corresponds to dividing the amplitude range of that given channel into 32 equivalent bins. Similar results were obtained with binning ranging from 8 to 128 bins.
- (2) The time series were compressed using the compressLib library for Matlab, this library implements the gzip algorithm to compress Matlab variables.
- (3) K(x) was calculated as the size of the compressed variable with time series divided by the size of the original variable. Our premise is that, the bigger the size of the compressed string, the more complex the structure of the time series, thus potentially indexing the complexity of the local neural processing captured by that sensor

Information sharing (across electrodes)

All information sharing measures were computed on a spatial Laplacian transformation of the EEG - a computation also known as Current Source Density (CSD) estimate (Kayser and Tenke, 2006).

Phase Lag Index (PLI)

The Phase Lag Index (PLI), initially proposed by Stam, Nolte & Daffertshofer (Stam et al., 2007) measures the asymmetry in the distribution of phase differences between two signals. We computed PLI using a series of traditional steps: (1) For each frequency-bin of interest (f, in δ [1-4 Hz], θ [4-8 Hz], α [8-13 Hz], β [13-30 Hz] and γ [30-45 Hz]), each pair of electrodes, and at each trial, the signal X and Y were band-passed filtered at *f*. (2) Then we applied the Hilbert-transformation to estimate the instantaneous phase $\varphi(\tau)$ and amplitude $\psi(\tau)$ of X and Y at each time point τ. (3) The phase difference (φ_Δ) between the two signals X and Y was then calculated as:

$$\varphi_{\Delta}(\tau) = \varphi_x(\tau) - \varphi_y(\tau)$$

Finally, the sign of the angle of the difference between $\varphi_x(\tau)$ and $\varphi_y(\tau)$ was calculated, and averaged across time.

$$PLI = \left| \frac{1}{N} \sum_{\tau} sign\left(\varphi_{\Delta}(\tau)\right) \right|$$

The mean PLI was calculated for each trial, and then averaged across trials. Note that although PLI is related to Phase Locking Value (PLV (Lachaux et al., 1999)), PLV can more easily conclude that two EEG electrodes are synchronized, because it is sensitive to common sources. By contrast, the PLI is insensitive to perfect, zero-phase synchrony and therefore focuses on connectivity between two electrodes which does not originate from a single common source. Finally, because the PLI is signed across pairs of electrodes, when we needed a summary value of PLI across electrode pairs, we averaged the absolute value of PLI.

weighted Symbolic Mutual Information

In order to quantify the coupling of information flow between electrodes we computed the weighted symbolic mutual information (wSMI, (J.-R. King et al., 2013)). This method is based on the PE analysis and is calculated between each pair of electrodes, and for each trial, after the transformation of the time series into sequence of symbols (see methods for permutation entropy). Identically to PE, the symbolic transformation depends on the applied tau parameter (in our case: τ = 8, 4, 2, 1 time sample(s) corresponding to $wSMI_{\theta}$, $wSMI_{\alpha}$, $wSMI_{\beta}$ and $wSMI_{\gamma}$). Then, wSMI was estimated for each pair of transformed EEG signals by estimating the joint probability of each pair of symbols. The joint probability matrix was multiplied by binary weights to reduce spurious correlations between signals. The weights were set to zero for pairs of identical symbols, which could be elicited by a unique common source, and for opposed symbols, which could reflect the two sides of a single electric dipole. wSMI is calculated using the following formula:

$$wSMI(X,Y) = \frac{1}{\log n!} \sum_{x \in X} \sum_{y \in Y} w(x,y)\, p(x,y) \log\left(\frac{p(x,y)}{p(x)p(y)}\right)$$

where *n* is the size of the vector used for the symbolic transformation, *x* and *y* are all symbols present in signals *X* and *Y* respectively, w*(x,y)* is the weight matrix and *p(x,y)* is the joint probability of co-occurrence of symbol *x* in signal *X* and symbol *y* in signal *Y*. Finally *p(x)* and *p(y)* are the probabilities of those symbols in each signal.

Multivariate Pattern Analyses computation

Multivariate Pattern Analyses (MVPAs) have proven to be an efficient neuroimaging tool to combine multiple sources of evidence within a single test (Haynes, 2011). In our case we implemented the MVPA to automatically classify the state of consciousness of each patient.

A support vector classification (SVC) method was used to distinguish VS from MCS patients. As described in the ERP decoding section, the SVC aims at finding the optimal linear combination of features (w) that separates the training samples with

distinct classes in the hyperspace of features. As there are more features than samples ($f >> n$), there is an infinity of possible w. A penalization parameter is thus used to find a solution which is likely to generalize to another dataset, and hence avoid over-fitting. Here, the penalization parameter C, was chosen by nested cross-validation among the values = [.001 .01 .1 .2 .5 1 2 10] using a grid-search method (Pedregosa et al., 2011) nested in the cross-validation (see below).

The SVC can provide a continuous probability by fitting the distribution of the samples with regard to w (Platt, 1999). To do so, a sigmoid function is fitted from the distributions of the signed distances separating the train samples and w. This sigmoid fit is then used to monotonically transform the signed distance separating the test samples and w into a meaningful probability(Platt, 1999).

The data provided to the classifier corresponds to the 92 EEG measures, topographically summarized as the mean and the standard deviation across non-facial electrodes. Similarly to topographical analyses, connectivity measures were first averaged as the median value each electrode shared with all other non-facial electrodes, and subsequently summarized as the mean and standard deviation across these non-facial averages. The data provided to the classifier thus corresponded to a matrix X of n samples (EEG recordings) by f features (f = 92 EEG measures * 2 topographical summaries) and a vector y of n samples corresponding to subjects' states of consciousness (1: VS, 2: MCS).

The Support Vector Classifier (SVC) was repeatedly cross-validated with stratified k-folding (k=8). Cross validation is a method aiming at testing the performance of a predictive model. It consists in repeatedly fitting this model on a subset of the data (training set) and subsequently testing it on the remaining data (test set). Stratified k-folding consists in arranging the partitioning of the data so that training and test sets keep constant proportion of each category samples. Stratified folding thus aims to minimize fold-specific effects.

Within each fold, we applied two successive preprocessing steps fitted on the train samples and subsequently applied to the test samples. 1) Normalization of each feature (remove mean, divide by standard deviation). 2) Feature selection (best single feature or best 20%) based on F-tests.

The classifier is fitted on the train set and subsequently assigns, to each test sample, a continuous probability of belonging to each class (VS, MCS). To minimize folding effects, the predicted probabilities of each sample were averaged across 250 repetitions of the SVC, each using pseudo-randomly partitioned stratified folding.

All MVPAs analyses were performed with the Scikit-learn package (Pedregosa et al., 2011).

Area under the curve (AUC) analysis

The ROC plots the false positive rates (FPR) as a function of true positive rates (TPR). For example, in a comparison of the alpha power between CS and VS patients, one can observe the percentage of CS patients (TPR) who show a higher alpha power than an arbitrarily setup criterion C, and the corresponding percentage of VS patients (FPR). By testing all possible empirical criteria, we can draw the ROC curve and compute the AUC (see supplementary figure 5). Values higher than 50% means that CS

patients have on average higher alpha power than VS patients, and values lower than 50% implies that CS patients have lower alpha power than VS patients.

The AUC derived from the ROC curve provides a criterion-free estimate of the discrimination capacity of a given measure. However, in the clinic, it is often useful to report sensitivity and specificity, which require the definition of a criterion beyond which a patient is classified in one group versus the other. From the ROC curve, a criterion can be estimated using the Youden's index (J) (Youden, 1950). This is the point of the ROC curve that maximizes the distance between the curve and the diagonal. Using this criterion, sensitivity and specificity were calculated for each measure. This information is presented in supplementary tables S1 and S7.

Note that the estimates of statistical effect size are intrinsically problematic in mass-univariate analyses, as one tends to look at the effect size of significant tests only. However, the effect size itself is an estimate and thus subject to error. We decided to make all values available to the reader, but we stress that it would be incorrect to pick the best measure as this may overestimate its effects size (Kriegeskorte et al., 2009; Vul et al., 2009). Each measure is intrinsically high dimensional, as it was measured on each EEG electrode (n=256) or on each pair of EEG electrodes (n=32640). To sum up these large datasets, we thus summarized each multidimensional measures in a single value. ERP measures were summarized as the mean value observed in regions of interests traditionally used in the literature. Connectivity measures computed for each pair of EEG electrodes were summarized as follow: for each non-facial electrode, we computed the median value it shared with all other non-facial electrode. We then averaged these 224 values to summarize the amount of shared information across the scalp. All other measures were summarized by averaging the 224 values non-facial electrodes.

To account for the large number of statistical tests (n = 92 measures x 3 comparisons), statistical significance was systematically corrected for multiple comparison with a false discovery rate method (FDR at alpha=.05) across all measures and comparisons.

Supplementary Results

Automatic classification and recovery: comparison of EEG *versus the CRS-R scale*

To assess whether the recovery of the patients from the VS state could be predicted from the Coma Recovery Scale Revised (CRS-R) scores at the moment of clinical evaluation of consciousness, we compared the CRS-R between the clinical VS patients that did recover and the VS patients that did not recover. None of the CRS-R subscores or the full sum distinguished between the two groups (Mann-U Whitney, $p > 0.08$ for CRS1, $p > 0.24$ for CRS2, $p > 0.28$ for CRS3, $p > 0.60$ for CRS4, 1 for CRS5, $p > 0.35$ for CRS6 and $p > 0.55$ for sum of CRS-R subscores).

The analysis was then repeated but specifically compared clinically VS patients' CRS-R scores depending on whether they were classified by the SVC as "VS" or as "MCS". None of the CRS-R subscores could differentiate between these two groups. (Mann-U Whitney, $p > 0.07$ for CRS1, $p > 0.07$ for CRS2, $p > 0.26$ for CRS3, $p > 0.87$

for CRS4, 1 for CRS5[1], $p > 0.08$ for CRS6 and $p > 0.14$ for sum of CRS-R subscores). This shows that, none of the clinical descriptions assessed on the patients at the moment of the recording could predict the distinction done by the EEG-based classifier

[1] Since all VS patients have a score of zero in Subscore 5 of the CRS-R scale a comparison cannot be computed.

Supplementary References

Baars BJ. A cognitive theory of consciousness. Cambridge University Press; 1993.

Bandt C, Pompe B. Permutation Entropy: A Natural Complexity Measure for Time Series. Phys. Rev. Lett. 2002; 88: 1–4.

Bekinschtein TA, Dehaene S, Rohaut B, Tadel F, Cohen L, Naccache L. Neural signature of the conscious processing of auditory regularities. Proc. Natl. Acad. Sci. U. S. A. 2009; 106: 1672–7.

Cao Y, Tung W, Gao J, Protopopescu V, Hively L. Detecting dynamical changes in time series using the permutation entropy. Phys. Rev. E 2004; 70: 046217.

Casali AG, Gosseries O, Rosanova M, Boly M, Sarasso S, Casali KR, et al. A Theoretically Based Index of Consciousness Independent of Sensory Processing and Behavior. Sci. Transl. Med. 2013; 5: 198ra105–198ra105.

Chaitin G. Information-theoretic computation complexity. IEEE Trans. Inf. Theory 1974; 20: 10–15.

Chaitin G. The berry paradox. Complex Syst. Bin. Networks 1995

Chang C, Lin C. LIBSVM: a library for support vector machines. Computer (Long. Beach. Calif). 2001; 2: 1–30.

Chennu S, Noreika V, Gueorguiev D, Blenkmann A, Kochen S, Ibáñez A, et al. Expectation and attention in hierarchical auditory prediction. J. Neurosci. 2013; 33: 11194–205.

Dehaene S, Changeux J-P, Naccache L, Sackur J, Sergent C. Conscious, preconscious, and subliminal processing: a testable taxonomy. Trends Cogn. Sci. 2006; 10: 204–11.

Dehaene S, Changeux J-PJP. Experimental and theoretical approaches to conscious processing. Neuron 2011; 70: 200–227.

Dimitrov AG, Lazar AA, Victor JD. Information theory in neuroscience. J. Comput. Neurosci. 2011; 30: 1–5.

Faugeras F, Rohaut B, Weiss N, Bekinschtein T, Galanaud D, Puybasset L, et al. Event related potentials elicited by violations of auditory regularities in patients with impaired consciousness. Neuropsychologia 2012; 50: 403–18.

Faugeras F, Rohaut B, Weiss N, Bekinschtein TA, Galanaud D, Puybasset L, et al. Probing consciousness with event-related potentials in the vegetative state. Neurology 2011; 77: 264–8.

Fellinger R, Klimesch W, Schnakers C, Perrin F, Freunberger R, Gruber W, et al. Cognitive processes in disorders of consciousness as revealed by EEG time-frequency analyses. Clin. Neurophysiol. 2011; 122: 2177–84.

Finelli LA, Borbely AA, Achermann P. Functional topography of the human nonREM sleep electroencephalogram. Eur. J. Neurosci. 2001; 13: 2282–2290.

Fingelkurts AA, Fingelkurts AA, Bagnato S, Boccagni C, Galardi G. EEG oscillatory states as neuro-phenomenology of consciousness as revealed from patients in vegetative and minimally conscious states. Conscious. Cogn. 2012; 21: 149–69.

Fischer C, Luaute J, Adeleine P, Morlet D. Predictive value of sensory and cognitive evoked potentials for awakening from coma. Neurology 2004; 63: 669–673.

Fischer C, Luaute J, Morlet D. Event-related potentials (MMN and novelty P3) in permanent vegetative or minimally conscious states. Clin. Neurophysiol. 2010; 121: 1032–42.

Fries P. A mechanism for cognitive dynamics: neuronal communication through neuronal coherence. Trends Cogn. Sci. 2005; 9: 474–80.

Gaillard R, Dehaene S, Adam C, Clémenceau S, Hasboun D, Baulac M, et al. Converging intracranial markers of conscious access. PLoS Biol. 2009; 7: e1000061.

Garrett DD, Kovacevic N, McIntosh AR, Grady CL. Blood oxygen level-dependent signal variability is more than just noise. J. Neurosci. 2010; 30: 4914–21.

Gómez CM, Flores A, Ledesma A. Fronto-parietal networks activation during the contingent negative variation period. Brain Res. Bull. 2007; 73: 40–47.

Gosseries O, Schnakers C, Ledoux D, Vanhaudenhuyse A, Bruno M-A, Demertzi A, et al. Automated EEG entropy measurements in coma, vegetative state/unresponsive wakefulness syndrome and minimally conscious state. Funct. Neurol. 2011; 26: 25–30.

Gross J, Schmitz F, Schnitzler I, Kessler K, Shapiro K, Hommel B, et al. Modulation of long-range neural synchrony reflects temporal limitations of visual attention in humans. Proc. Natl. Acad. Sci. U. S. A. 2004; 101: 13050–5.

Haynes J-D. Multivariate decoding and brain reading: introduction to the special issue. Neuroimage 2011; 56: 385–6.

Hipp JF, Engel AK, Siegel M. Oscillatory synchronization in large-scale cortical networks predicts perception. Neuron 2011; 69: 387–96.

Inouye T, Shinosaki K, Sakamoto H, Toi S, Ukai S, Iyama A, et al. Quantification of EEG irregularity by use of the entropy of the power spectrum. Electroencephalogr. Clin. Neurophysiol. 1991; 79: 204–210.

Jordan D, Stockmanns G, Kochs EF, Pilge S, Schneider G. Electroencephalographic order pattern analysis for the separation of consciousness and unconsciousness: an analysis of approximate entropy, permutation entropy, recurrence rate, and phase coupling of order recurrence plots. Anesthesiology 2008; 109: 1014–22.

Kayser J, Tenke CE. Principal components analysis of Laplacian waveforms as a generic method for identifying ERP generator patterns: I. Evaluation with auditory oddball tasks. Clin. Neurophysiol. 2006; 117: 348–68.

King JR, Faugeras F, Gramfort A, Schurger A, El Karoui I, Sitt JD, et al. Single-trial decoding of auditory novelty responses facilitates the detection of residual consciousness. Neuroimage 2013; 83C: 726–738.

King J-R, Sitt JD, Faugeras F, Rohaut B, El Karoui I, Cohen L, et al. Information Sharing in the Brain Indexes Consciousness in Noncommunicative Patients. Curr. Biol. 2013; 23: 1914–1919.

Kolmogorov A. Three approaches to the quantitative definition of information. Probl. Inf. Transm. 1965; 1: 1 – 7.

Kotchoubey B, Lang S, Mezger G, Schmalohr D, Schneck M, Semmler A, et al. Information processing in severe disorders of consciousness: vegetative state and minimally conscious state. Clin. Neurophysiol. 2005; 116: 2441–53.

Kriegeskorte N, Simmons WK, Bellgowan PSF, Baker CI. Circular analysis in systems neuroscience: the dangers of double dipping. Nat. Neurosci. 2009; 12: 535–40.

Lachaux JP, Rodriguez E, Martinerie J, Varela FJ. Measuring phase synchrony in brain signals. Hum. Brain Mapp. 1999; 8: 194–208.

Laitio RM, Kaskinoro K, S\"arkel\"a MOK, Kaisti KK, Salmi E, Maksimow A, et al. Bispectral index, entropy, and quantitative electroencephalogram during single-agent xenon anesthesia. Anesthesiology 2008; 108: 63.

Laureys S, Owen AM, Schiff ND. Brain function in coma, vegetative state, and related disorders. Lancet Neurol. 2004; 3: 537–46.

Lehembre R, Marie-Aurélie B, Vanhaudenhuyse A, Chatelle C, Cologan V, Leclercq Y, et al. Resting-state EEG study of comatose patients: a connectivity and frequency analysis to find differences between vegetative and minimally conscious states. Funct. Neurol. 2012; 27: 41–7.

Lempel A, Ziv J. On the Complexity of Finite Sequences. IEEE Trans. Inf. Theory 1976; 22: 75–81.

Li X, Cui S, Voss LJ. Using permutation entropy to measure the electroencephalographic effects of sevoflurane. Anesthesiology 2008; 109: 448–56.

MacKay DJC. Information Theory, Inference and Learning Algorithms. Cambridge University Press; 2003.

Mitra P, Bokil H. Observed Brain Dynamics. Oxford University Press, USA; 2007.

Morlet D, Fischer C. MMN and Novelty P3 in Coma and Other Altered States of Consciousness: A Review. Brain Topogr. 2013

Näätänen R, Gaillard AWK, Mäntysalo S. Early selective-attention effect on evoked potential reinterpreted. Acta Psychol. (Amst). 1978; 42: 313–329.

Naccache L, Puybasset L, Gaillard R, Serve E, Willer J-C. Auditory mismatch negativity is a good predictor of awakening in comatose patients: a fast and reliable procedure. Clin. Neurophysiol. 2005; 116: 988–9.

Nashida T, Yabe H, Sato Y, Hiruma T, Sutoh T, Shinozaki N, et al. Automatic auditory information processing in sleep. Sleep 2000; 23: 821–828.

Niedermeyer E. Electrophysiology of the frontal lobe. Clin. Electroencephalogr. 2003; 34: 5–12.

Nolte G, Bai O, Wheaton L, Mari Z, Vorbach S, Hallett M. Identifying true brain interaction from EEG data using the imaginary part of coherency. Clin. Neurophysiol. 2004; 115: 2292–2307.

Pedregosa F, Varoquaux G, Gramfort A, Michel V, Thirion B, Grisel O, et al. Scikit-learn: Machine Learning in Python. J. Mach. Learn. Res. 2011; 12: 2825–2825–2830–2830.

Platt JC. Probabilistic Outputs for Support Vector Machines and Comparisons to Regularized Likelihood Methods. Adv. large margin Classif. 1999; 10: 61–174.

Polich J. Updating P300: An integrative theory of P3a and P3b. Clin. Neurophysiol. 2007; 118: 2128–2148.

Rampil IJ. A primer for EEG signal processing in anesthesia. Anesthesiology 1998; 89: 980–1002.

Rees G, Kreiman G, Koch C. Neural correlates of consciousness in humans. Nat. Rev. Neurosci. 2002; 3: 261–70.

Rosahl SK, Knight RT. Role of Prefrontal Cortex in Generation of the Contingent Negative Variation. Cereb. Cortex 1995; 5: 123–134.

Saalmann YB, Pinsk MA, Wang L, Li X, Kastner S. The pulvinar regulates information transmission between cortical areas based on attention demands. Science 2012; 337: 753–6.

Salomon D. Data Compression: The Complete Reference (Vol. 10). Springer-Verlag; 2007.

Schnakers C, Ledoux D, Majerus S, Damas P, Damas F, Lambermont B, et al. Diagnostic and prognostic use of bispectral index in coma, vegetative state and related disorders. Brain Inj. 2008; 22: 926–31.

Schnakers C, Perrin F, Schabus M, Hustinx R, Majerus S, Moonen G, et al. Detecting consciousness in a total locked-in syndrome: an active event-related paradigm. Neurocase 2009; 15: 271–7.

Sergent C, Baillet S, Dehaene S. Timing of the brain events underlying access to consciousness during the attentional blink. Nat. Neurosci. 2005; 8: 1391–400.

Sergent C, Naccache L. Imaging neural signatures of consciousness: “What”, “When”, “Where” and “How” does it work? Arch. Ital. Biol. 2012; 150: 91–106.

Shaw FZ, Chen RF, Tsao HW, Yen CT. Algorithmic complexity as an index of cortical function in awake and pentobarbital-anesthetized rats. J. Neurosci. Methods 1999; 93: 101–10.

Squires NK, Squires KC, Hillyard SA. Two varieties of long-latency positive waves evoked by unpredictable auditory stimuli in man. Electroencephalogr. Clin. Neurophysiol. 1975; 38: 387–401.

Stam CJ, Nolte G, Daffertshofer A. Phase lag index: assessment of functional connectivity from multi channel EEG and MEG with diminished bias from common sources. Hum. Brain Mapp. 2007; 28: 1178–93.

Stam CJ. Nonlinear dynamical analysis of EEG and MEG: review of an emerging field. Clin. Neurophysiol. 2005; 116: 2266–301.

Supp GG, Siegel M, Hipp JF, Engel AK. Cortical hypersynchrony predicts breakdown of sensory processing during loss of consciousness. Curr. Biol. 2011; 21: 1988–93.

Tononi G. Consciousness as Integrated Information: a Provisional Manifesto. Biol. Bull. 2008; 215: 216–242.

Vakkuri A, Yli-Hankala A, Talja P, Mustola S, Tolvanen-Laakso H, Sampson T, et al. Time-frequency balanced spectral entropy as a measure of anesthetic drug effect in central nervous system during sevoflurane, propofol, and thiopental anesthesia. Acta Anaesthesiol. Scand. 2004; 48: 145–153.

Velly LJ, Rey MF, Bruder NJ, Gouvitsos F a, Witjas T, Regis JM, et al. Differential dynamic of action on cortical and subcortical structures of anesthetic agents during induction of anesthesia. Anesthesiology 2007; 107: 202–12.

Viertiö-Oja H, Maja V, Särkelä M, Talja P, Tenkanen N, Tolvanen-Laakso H, et al. Description of the Entropy algorithm as applied in the Datex-Ohmeda S/5 Entropy Module. Acta Anaesthesiol. Scand. 2004; 48: 154–61.

Vogt F, Klimesch W, Doppelmayr M. High-frequency components in the alpha band and memory performance. J. Clin. Neurophysiol. 1998; 15: 167–72.

Vul E, Harris C, Winkielman P, Pashler H. Puzzlingly High Correlations in fMRI Studies of Emotion, Personality, and Social Cognition. Perspect. Psychol. Sci. 2009; 4: 274–290.

Walter WG, Cooper R, Aldrige VJ, Mccallum WC, Winter AL. Contingent negative variation : An electric sign of sensori-motor association and expectancy in the human brain. Nature 1964; 203: 380–384.

Welch P. The use of fast Fourier transform for the estimation of power spectra: A method based on time averaging over short, modified periodograms. IEEE Trans. Audio Electroacoust. 1967; 15: 70–73.

Wijnen VJM, van Boxtel GJM, Eilander HJ, de Gelder B. Mismatch negativity predicts recovery from the vegetative state. Clin. Neurophysiol. 2007; 118: 597–605.

Youden WJ. Index for rating diagnostic tests. Cancer 1950; 3: 32–35.

Supplementary figures

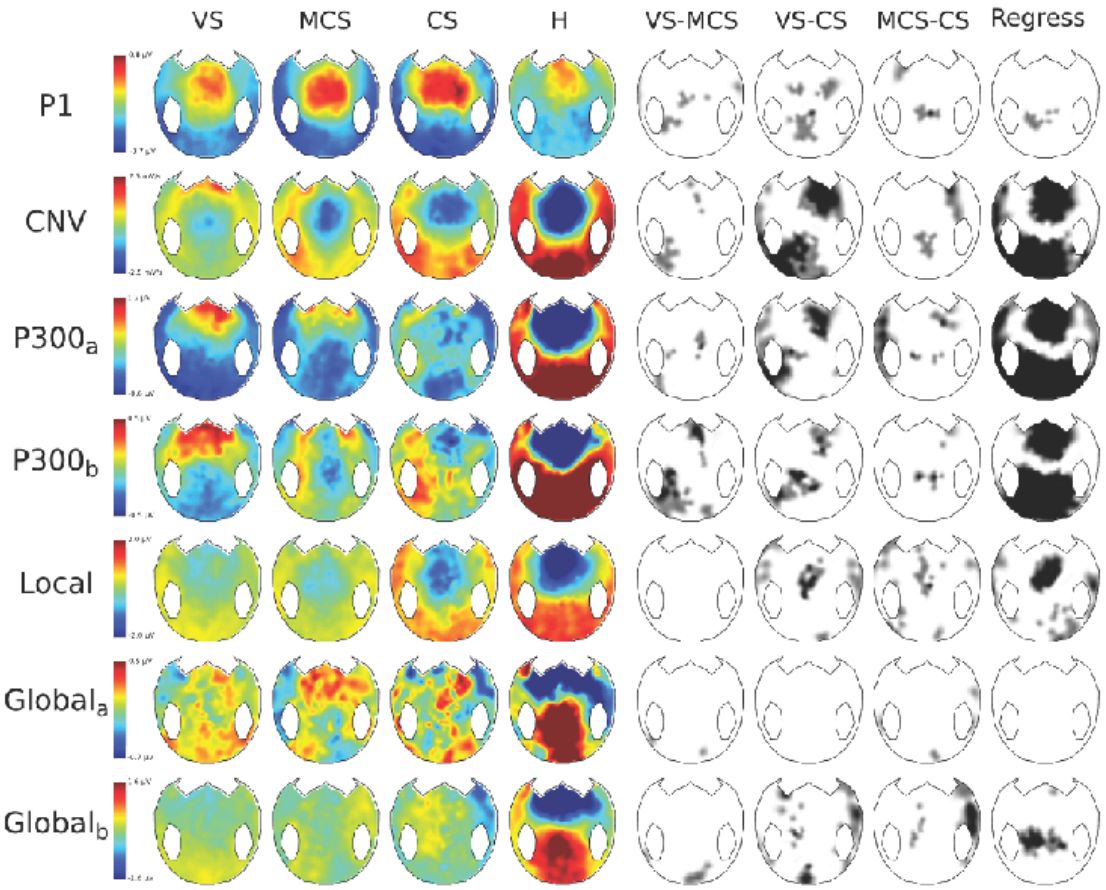

Figure S1. Scalp topography of all computed EEG event related potentials (ERPs) measures

The topographical 2D projection (top = front) of each measure is plotted for each state of consciousness (columns 1 = VS, 2 = MCS, 3 = CS, 4 = Healthy control = CS). The fifth to seventh column indicates whether significant differences were observed across these states (black = $P < 0.01$, light grey = $P < 0.05$, white = n.s., uncorrected for the number of electrodes tested). The eight column shows the statistics of a regression analysis of the measure across the four states of consciousness (VS<MCS<CS<Healthy controls. black = $P < 0.01$, light grey = $P < 0.05$, white = n.s., uncorrected for the number of electrodes tested).

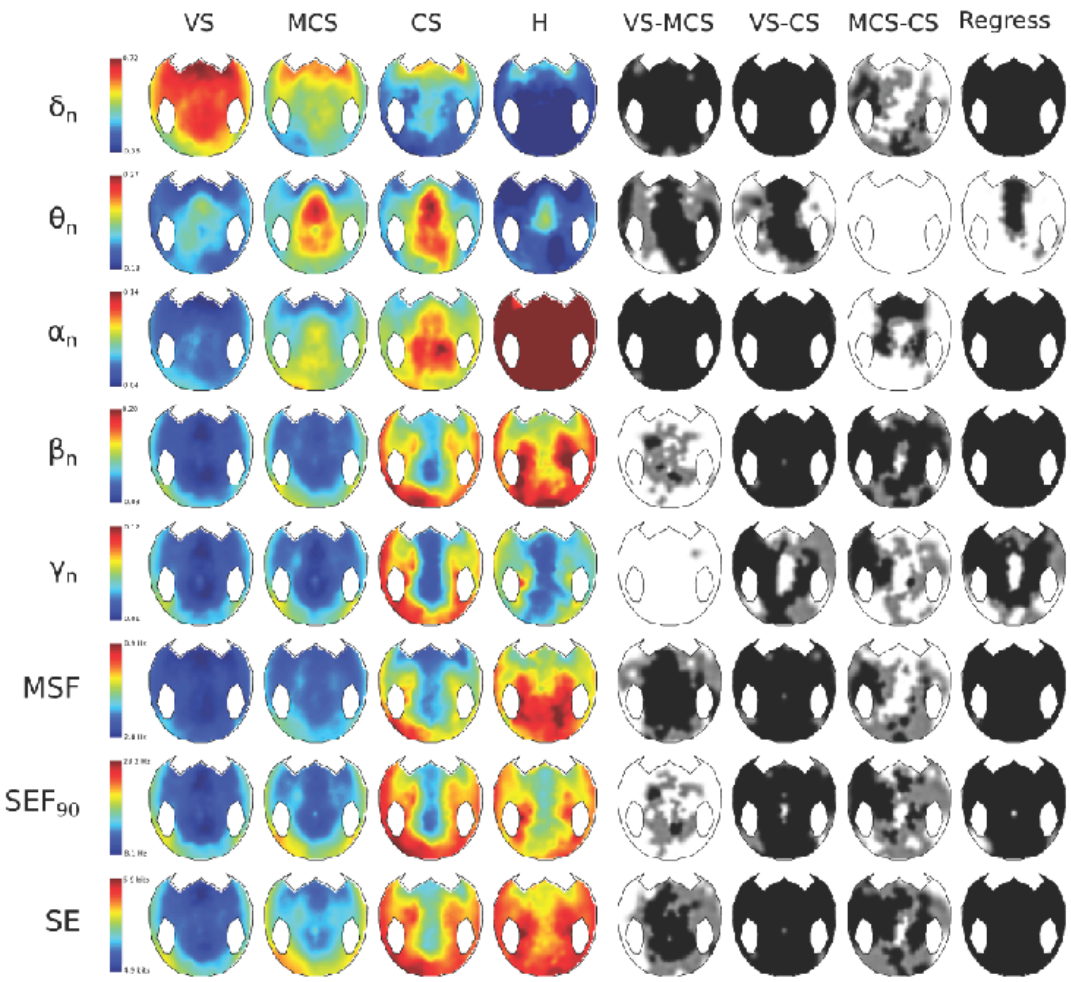

Figure S2. Scalp topography of all computed EEG spectral measures

The topographical 2D projection (top = front) of each spectral measure is plotted for each state of consciousness following the same nomenclature as in Figure S1.

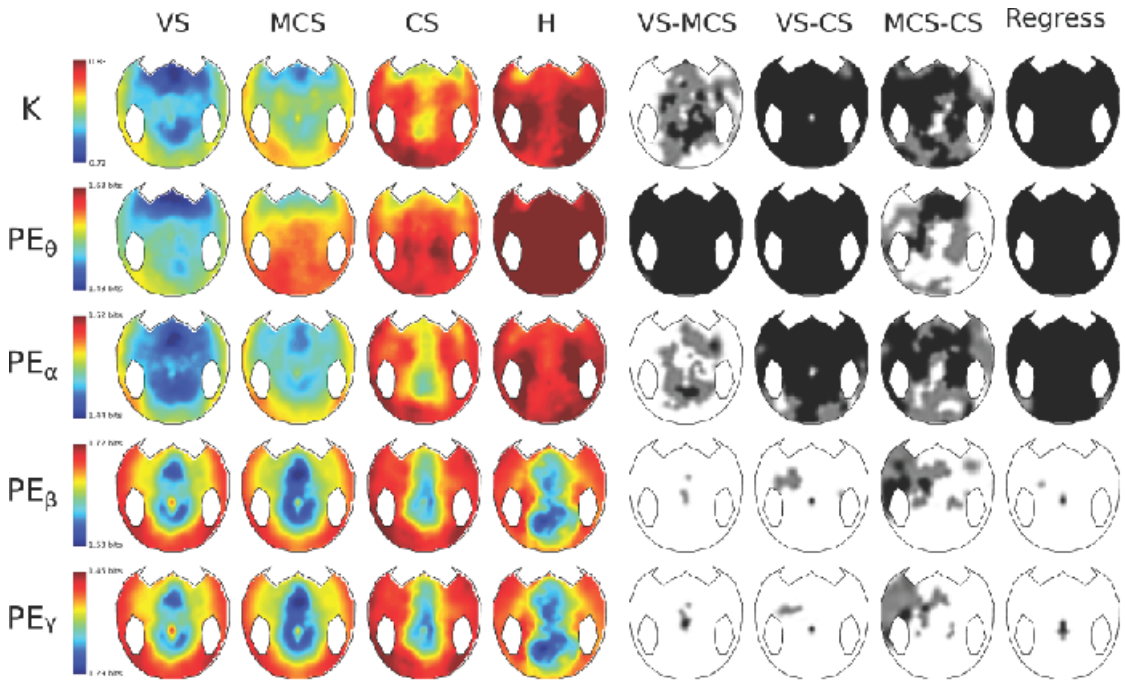

Figure S3. Scalp topography of all computed EEG complexity measures

The topographical 2D projection (top = front) of each complexity measure is plotted for each state of consciousness following the same nomenclature as in Figure S1.